Characterization of $Ar_nCl^{(-)}$ clusters ($n=2-15$) using zero electron kinetic energy and partially discriminated threshold photodetachment spectroscopy

Thomas Lenzer,[a] Ivan Yourshaw, Michael R. Furlanetto,[b] Nicholas L. Pivonka, and Daniel M. Neumark[c]
Department of Chemistry, University of California, Berkeley, California 94720 and Chemical Sciences Division, Lawrence Berkeley National Laboratory, Berkeley, California 94720

(Received 23 April 2001; accepted 6 June 2001)

Ar_nCl^- clusters have been investigated by anion zero electron kinetic energy (ZEKE) and partially discriminated threshold photodetachment spectroscopy. The experiments yield size-dependent electron affinities (EAs) and electronic state splittings for the *X*, *I*, and *II* states accessed by photodetachment. Cluster minimum energy structures have been determined from calculations based on a ''simulated annealing'' approach employing our recently presented $Ar–Cl^{(-)}$ pair potentials from anion ZEKE spectroscopy [T. Lenzer, I. Yourshaw, M. R. Furlanetto, G. Reiser, and D. M. Neumark, J. Chem. Phys. **110**, 9578 (1999)] and various nonadditive terms. The EAs calculated without many-body effects overestimate the experimental EAs by up to 1500 cm^{-1}. Repulsive many-body induction in the anion clusters is found to be the dominant nonadditive effect. In addition, the attractive interaction between the chloride charge and the Ar_2 exchange quadrupole is important. These findings are consistent with our earlier results for Xe_nI^-, Ar_nI^-, and Ar_nBr^- clusters and highlight again the necessity of an adequate implementation of many-body effects to describe the energetics of such systems. For Ar_nCl^- clusters with $n>12$ we find some deviations between experimental and calculated (0 K) EA which can be explained by the population of less stable anion structures due to the finite temperatures of the clusters in our experiments. This results in lower EAs than predicted for the corresponding global minimum energy structures. © *2001 American Institute of Physics.* [DOI: 10.1063/1.1388202]

I. INTRODUCTION

The reaction dynamics and photophysics of charged and neutral atomic and molecular species in solution, matrices, crystals, and clusters is crucially influenced by weak interactions with the surrounding atoms or molecules.[1–5] In an attempt to systematically characterize such interactions in detail, we have recently carried out a series of experimental studies on rare gas halide clusters (Rg_nX^-) as model systems. In these investigations the halide ion X^- in the cluster was probed by high resolution anion threshold photodetachment spectroscopy. Species ranging from binary complexes[6–9] up to large clusters[10,11] have been studied so far. In this work, we extend our experiments to Ar_nCl^- clusters, with the goal of assessing the influence of many-body effects on the structure and energetics of these species.

The simplest description of weak interactions in a system of *N* particles assumes only *pairwise additivity* of the atom–atom interactions V_{ij},

$$V_{\mathrm{p}}=\sum_{i<j}^{N} V_{ij}(|\mathbf{r}_i-\mathbf{r}_j|). \tag{1}$$

Here, $\mathbf{r}_i$ and $\mathbf{r}_j$ denote the positions of two individual atoms. However, in reality the situation is much more complex due to the presence of dispersion, induction, and exchange interactions.[12] Therefore it is necessary to go beyond Eq. (1) and include nonadditive interactions of the type,

$$V_{\text{many-body}}=\sum_{i<j<k}^{N} V_{ijk}(\mathbf{r}_i,\mathbf{r}_j,\mathbf{r}_k)+\cdots + \sum_{i<j<k<\ldots<z}^{N} V_{ijk\cdots z}(\mathbf{r}_i,\mathbf{r}_j,\mathbf{r}_k,\ldots,\mathbf{r}_z). \tag{2}$$

Anion zero electron kinetic energy (ZEKE) spectroscopy and partially discriminated threshold photodetachment (PDTP) have proved to be useful tools to investigate such many-body effects in negative ion clusters. Here we present an experimental study of Ar_nCl^- clusters with up to fifteen argon atoms. ZEKE spectroscopy combines mass-selectivity with sufficient spectroscopic resolution (typically 1–2 cm^{-1} for atomic systems[11]). It is therefore possible to extract precise electron affinities (EAs) and characterize the electronic structure of the neutral clusters accessed by photodetachment. We have already demonstrated this in our earlier studies of diatomic[6–9] and polyatomic[10,11,13] rare gas halides. The latter studies on Xe_nI^- ($n=2-14$), Ar_nI^- ($n=2-19$), and Ar_nBr^- ($n=2-9$) allowed us to characterize the many-body effects in these systems in considerable detail.

[a]Current address: Institut für Physikalische Chemie, Universität Göttingen, Tammannstraße 6, D-37077 Göttingen, Germany.
[b]National Science Foundation Predoctoral Fellow.
[c]Author to whom correspondence should be addressed. Fax: +01-510-642-3635; electronic mail: dan@radon.cchem.berkeley.edu

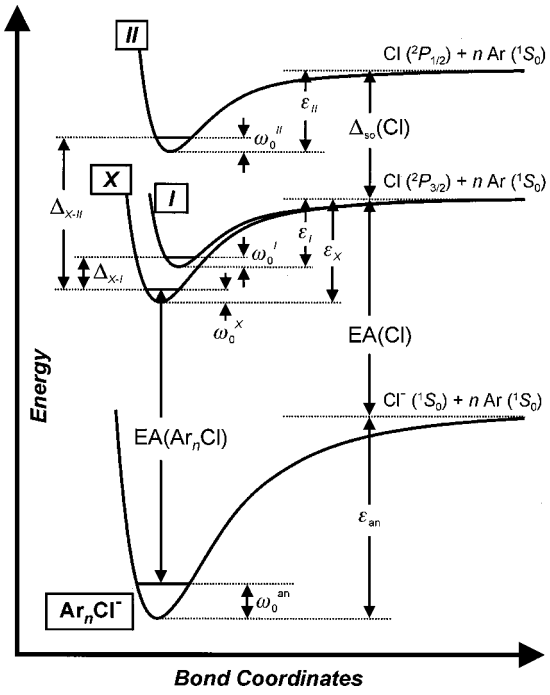

FIG. 1. Scheme of the potential energy levels involved in the photodetachment of Ar_nCl^- clusters. The energetic relations among the atomic and molecular anion and neutral electronic states are shown. For a description of the various quantities, see Sec. IV.

Whereas our most recent study on Xe_nI^- clusters dealt with species having particularly large polarizabilities, the present experiments focus on another ''extreme'' case, Ar_nCl^- clusters, in which the atoms are considerably smaller and much less polarizable. At the same time, because of the smaller diameter of the Cl^- ion (compared to the I^- ion), the charge density of the anion is significantly increased. Together with our earlier studies we have now covered a fairly broad range of systems, allowing us to deduce general trends and give recommendations for modeling the interactions in all of these and related systems. In addition, some of the clusters studied here, especially the smaller Ar_nCl^- species, might serve as benchmark systems for *ab initio* methods. The first promising attempts in this direction have already been carried out for Ar_2Cl^-.[14]

By photodetachment we access the neutral Ar_nCl clusters. A unique class of ''nonadditive effects'' is present solely in these species due to the open-shell nature of the chlorine atom. This interaction leads to three doubly degenerate neutral electronic states (denoted as *X*, *I*, and *II*), as shown in the potential scheme of Fig. 1. All these states can be accessed by photodetachment of the respective Ar_nCl^- anion, thereby allowing us to characterize the splitting between the different neutral Ar_nCl states as a function of cluster size. Such information on the different neutral potential surfaces is important for investigating nonadiabatic processes in the condensed phase such as the relaxation of spin–orbit excited chlorine atoms in solid argon.[15] Other applications include molecular dynamics simulations of chlorine atoms on argon surfaces as model systems, with possible implications for photodeposition, photoetching, and photodoping processes.[16,17] Our results are also relevant for interpreting time-resolved emission experiments for the dissociation of Cl_2 in solid Ar.[18] Finally, our experimental data may be used to construct improved empirical potential surfaces for other species as, e.g., Ar_nCl_2 clusters[19] which have served as benchmark experimental systems for studying van der Waals interactions.[20–22]

From our earlier study of $ArCl^-$ we deduced two-body $Ar–Cl^{(-)}$ anion and neutral potential functions *via* vibrationally resolved ZEKE spectroscopy.[9] Very recently, these results have been confirmed by Boesl and co-workers using the same experimental technique.[23] On the basis of our pair potentials we can predict binding energies and structures of the larger anion and neutral $Ar_nCl^{(-)}$ clusters, and then compare these predictions with the experimental EAs. As was seen in our results for other polyatomic rare gas halogen systems, the simple ''additive picture'' [Eq. (1)] is inadequate. Therefore we systematically investigate how the inclusion of various many-body effects affects the calculated EAs, and ultimately find good agreement with experiment with virtually no adjustable parameters.

Our paper is organized as follows: Section II contains a brief discussion of the experimental details relevant for studying Ar_nCl^- anions. In Sec. III we present our ZEKE and PDTP spectra and assign the spectral features. Section IV gives more details about the two-body and three-body potential functions used in the simulations of our experimental data, and specific information on the MD calculations used for calculating the cluster structures is provided. In Sec. V we analyze and discuss our experimental findings: the electron affinities and the splittings between the neutral *X*, *I*, and *II* states are compared with the predictions of the model potentials, allowing us to quantify the influence of individual many-body effects. We finally consider the possible influence of internal excitation of the clusters on the experimental EAs.

II. ZEKE AND PDTP EXPERIMENTS

The anion ZEKE spectrometer has been described in detail elsewhere.[9,24,25] Here we only consider the specific details relevant to the present study. Ar_nCl^- anions are generated in the following way: argon is passed over CCl_4 (cooled to 0 °C) and then expanded into a vacuum through a 0.5 mm aperture in a pulsed valve (General Valve Series 9). Typical backing pressures are 60–130 psig. A 1 keV electron beam crosses the expansion just in front of the valve. Negative cluster ions are formed by dissociative attachment of low energy secondary electrons to CCl_4 and subsequent clustering of the Cl^- anions in the continuum flow region of the free-jet expansion. Cooling of the Ar_nCl^- clusters takes place as the expansion progresses. After passing through two skimmers[8,9] into a differentially pumped region, the clusters are accelerated to 1 keV. Mass-selection is achieved in a 1 m collinear time-of-flight mass spectrometer.

Upon entering the detector region, Ar_nCl^- anions of the desired mass are photodetached by an excimer-pumped dye laser (Lambda Physik EMG 202 and FL 3002). For photodetachment to the *X*, *I*, and *II* states (see Fig. 1) PTP, Rhodamine 640, Rhodamine 610, and Rhodamine 590 dyes are used (all from Exciton). For the Rhodamine dyes the

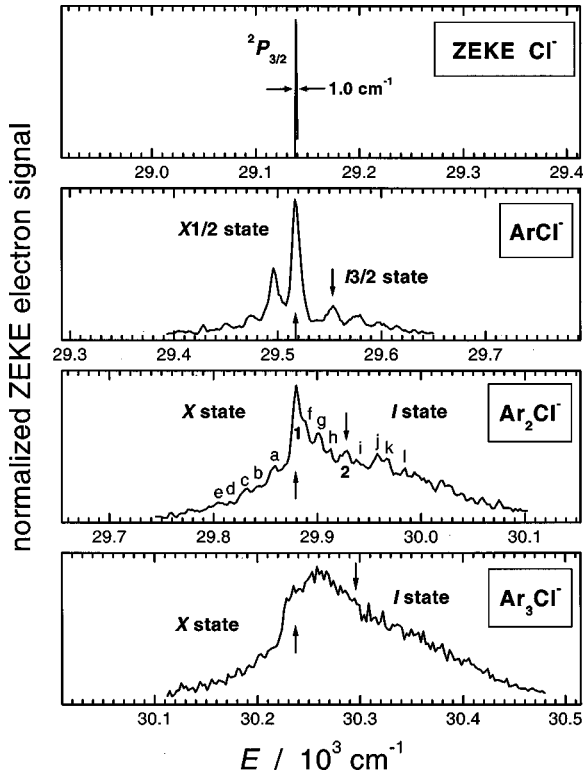

FIG. 2. $^2P_{3/2}$ state ZEKE spectrum for chloride and $X+I$ state ZEKE spectra for $ArCl^-$, Ar_2Cl^-, and Ar_3Cl^-. Arrows in the Ar_nCl^- spectra mark positions of the 0–0 transition for the X and I state of each cluster (partly estimated). For discussion of the marked $X+I$ state features in the Ar_2Cl^- spectrum, see the text.

output is frequency doubled in a KDP crystal. The typical laser energy range is 2–30 mJ/pulse. As in our earlier studies a weak dc field of -15 mV/cm is applied across the electron detachment region at all times. This enhances the electron signal considerably.[8] Also as in our earlier studies,[10,11] two different modes of electron detection are used: the higher resolution ZEKE mode, and the lower resolution partially discriminated threshold photodetachment (PDTP) mode.

In the ZEKE mode, after a delay of 200–500 ns, the electrons are extracted coaxially with the ion beam. This is achieved by applying a pulsed extraction field of 4 V/cm across the extraction plates. The photoelectrons are then deflected to an off-axis MCP detector. Near-zero kinetic energy electrons are detected selectively through a combination of time-gated detection and spatial discrimination; the latter is achieved by a series of apertures between the detachment region and the detector.[24] The ultimate spectral resolution of the instrument is about 1.0 cm^{-1} for Cl^- (Fig. 2). The resolution of the cluster ZEKE spectra reported in this study is generally poorer than this limit due to unresolved rotational envelopes and ''hot band'' congestion. Also, in some cases somewhat shorter extraction delays than required for maximum resolution are used, resulting in more rapid data acquisition but a slight degradation in resolution. The performance of the ZEKE mode is routinely checked by optimizing the spectral resolution for the well-known systems Cl^- and $ArCl^-$ (see Fig. 2 and Ref. 9).

The PDTP mode can be thought of as a ''low resolution ZEKE'' mode. In this case there is *no* delay between photodetachment and electron extraction, i.e., the extraction field immediately accelerates all of the photoelectrons toward the detector. However, due to the presence of the apertures, spatial discrimination against those photoelectrons having a significant velocity component perpendicular to the ion beam axis can still be achieved. This ''partially discriminated'' mode is very similar to the ''steradiancy detector'' of Baer *et al.*[26] and Spohr *et al.*[27] Typical PDTP peaks have a widths of about 150 cm^{-1} for the conditions used in our study and an asymmetric shape, i.e., they tail off toward high electron kinetic energies. Electron affinities determined this way have an estimated accuracy of about ± 50 cm^{-1}. The PDTP mode has the advantage of much higher electron sensitivity than the ZEKE mode, though at the cost of up to two orders of magnitude in resolution.

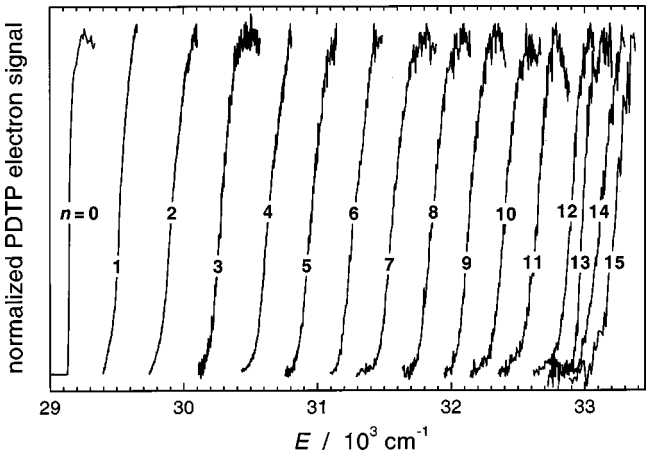

FIG. 3. The X and I state partially discriminated threshold photodetachment (PDTP) spectra for all Ar_nCl^- clusters studies ($n=0-15$). Note the considerably steeper slope of the PDTP curve for the $Ar_{13}Cl^-$ cluster compared to the other clusters of similar size.

The experiment is operated at a repetition rate of 30 Hz. The ZEKE (PDTP) spectra are normalized to the ion signal and laser power, and averaged over typically 1500–4000 (500–2000) laser shots per point. Absolute vacuum wavelengths are obtained by calibration of the dye laser either with a New Focus 7711 Fizeau wavelength meter or a Fe/Ne hollow cathode lamp.

III. ZEKE AND PDTP RESULTS

The ZEKE and PDTP spectra for the Ar_nCl^- clusters can be found in Figs. 2–4. As is evident from Fig. 1 and our earlier experiments on other diatomic and polyatomic $RgX^{(-)}$ species, we expect to observe two sets of features separated by approximately the spin–orbit splitting $\Delta_{so}(Cl)$ of atomic chlorine ($882.4\,cm^{-1}=109.4\,meV$).[28] The features at lower energy (Figs. 2 and 3) arise from transitions from the anion cluster to electronic states correlating with the $^2P_{3/2}$ ground state of the chlorine atom, and those at higher energy are due to transitions to states that correlate to the chlorine $^2P_{1/2}$ state (Fig. 4).

We first focus in detail on the ZEKE spectra for the low energy features. Figure 2 shows the ZEKE scans of this study taken for $n=0-3$. With increasing number of argon

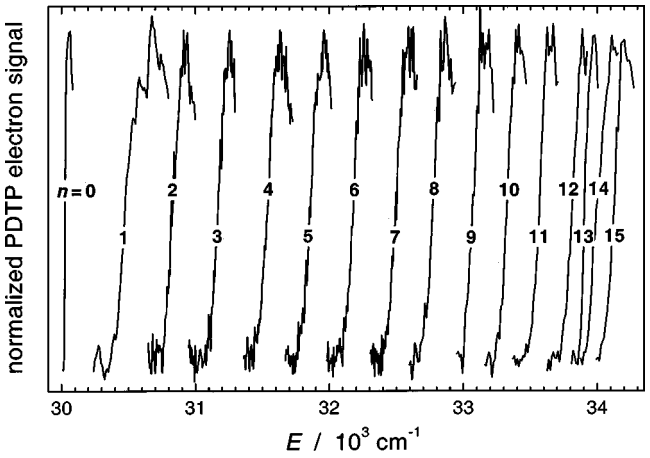

FIG. 4. As in Fig. 3, but for the *II* state.

atoms the spectra appear at increasingly higher energy, i.e., they are progressively blue shifted relative to the position of the Cl^- peak ($n=0$). This indicates that the anion clusters are more strongly bound than the neutral species.

The spectrum for Cl^- photodetachment to the $Cl(^2P_{3/2})$ state consists of a single peak at 29 138.6 cm^{-1}. This value is in excellent agreement with the current best value for EA(Cl), 29 138.59 cm^{-1} (from Ref. 29). To our knowledge the FWHM of 1.0 cm^{-1} we achieve is the best resolution obtained so far in an anion ZEKE experiment. Spectra for larger clusters ($n>0$) show features that stem from photodetachment to the *X* and *I* electronic states (see Fig. 1). Compared to our previous work on other diatomic rare gas iodide and rare gas bromide species,[6–8] as well as larger Xe_nI^-, Ar_nI^-, and Ar_nBr^- clusters[10,11] the *X* and *I* bands are much more closely spaced because of the considerably smaller $X-I$ splitting for the argon chlorine clusters [e.g., 36.6 cm^{-1} (ArCl) compared to 60.0 cm^{-1} (XeI)]. For the larger clusters with $n>2$, well separated *X* and *I* state bands [as, for example, in the case of Xe_nI^- (Ref. 11)] are therefore *not* observed because of this considerable overlap.

The $ArCl^-$ ZEKE spectrum was already discussed at length in our earlier study,[9] and therefore only a brief summary is given here. The largest peak in the spectrum (marked by an upward arrow in Fig. 2) corresponds to the 0–0 transition from the anion to the $X1/2$ neutral state. Peaks at lower energy with a spacing of approximately 21 cm^{-1} are due to sequence band transitions from vibrationally excited levels of the anion. *I* state transitions start above 29 540 cm^{-1}. In Fig. 2 the position of the $I3/2\leftarrow$anion 0–0 transition is marked by a downward arrow. The spacing between the two arrows directly yields an accurate $X-I$ splitting of 36.6 cm^{-1} for ArCl.

The Ar_2Cl^- ZEKE spectrum is broader than that of $ArCl^-$, though the band envelope is similar. The spectrum is dominated by a sharp peak at 29 879.7 cm^{-1} denoted as **1**. In analogy to $ArCl^-$, we assign it to the 0–0 transition from the anion to the *X* state which yields an accurate adiabatic EA for Ar_2Cl. There are some partially resolved peaks ("a"···"e") visible between 29 800 cm^{-1} and 29 860 cm^{-1}. They are spaced by about 10–15 cm^{-1} to the red of peak **1**. Their location at energies lower than the 0–0 transition identifies these peaks as sequence band transitions. As the $X-I$ splitting is fairly small, one expects transitions to the *X* and *I* states to overlap, particularly just to the blue of peak **1**. Thus, for peaks "f" to "h," no definite assignments to either the *X* or the *I* state can be given. Further to the blue, we tentatively assign peak **2** as the 0–0 transition to the *I* state on the basis of the $X-I$ splitting obtained from our MD simulations (Sec. V). Peaks at even higher energies ("i"–"l") probably belong to the *I* state.

The ZEKE spectra for larger *n* are broader still, and no particularly sharp peaks can be found. For example, in the Ar_3Cl^- spectrum (Fig. 2) only the location of the 0–0 transition to the *X* state can be estimated based on the abrupt rise in the ZEKE cross section. The approximate location of the *I* state 0–0 transition can be tentatively assigned using the $X-I$ splitting obtained in our MD simulations. The observed spectral congestion suggests some degree of vibrational excitation in the Ar_nCl^- anions.

Another interesting point concerns the relative intensities of the *X* and *I* state features, which change considerably with cluster size. For the $ArCl^-$ diatomic the *I* state is considerably weaker than the *X* state (Fig. 2).[9] However, the relative intensity of the *I* state increases for $n=2$ and 3. This trend is similar to that observed in the ZEKE spectra of Xe_nI^- clusters.[11]

The *X* and *I* state ZEKE spectra for clusters with $n>3$ became even more congested and no clearly resolved peaks could be found. For this reason, we only used the PDTP mode, which yields considerably higher electron signals. The results for $n=0-15$ are presented in Fig. 3. For the sake of clarity, only the rising edge of each PDTP signal is shown. Typically, the PDTP spectrum rises sharply at threshold up to a maximum and then tails off toward higher energies. We obtain a FWHM of 150 cm^{-1} in PDTP mode. This was routinely checked for the chlorine PDTP spectrum by monitoring the transition to the $^2P_{3/2}$ spin–orbit state.

In analogy to the ZEKE spectra in Fig. 2, the PDTP spectra appear at increasingly higher energy with increasing number of argon atoms, i.e., they are progressively blue shifted. The blue shift between $Ar_{11}Cl^-$ and $Ar_{12}Cl^-$ is comparable to that between $n=10$ and 11. In contrast, the PDTP spectrum for $Ar_{13}Cl^-$ appears at only slightly higher energies than for $Ar_{12}Cl^-$. It is also much steeper than the PDTP spectra of the other clusters in this size regime. While at first glance this might be associated with the closing of the first shell of argon atoms around the chloride anion at $n=12$, MD simulations between 0 and 60 K presented in Sec. V will show that the situation is more complicated.

We next consider the Ar_nCl^- *II* state spectra. Here, we could only obtain a well-resolved spectrum for $ArCl^-$ ($n=1$), which was already discussed in our earlier paper.[9] Spectra for $n>1$ were broad and unstructured. Thus for clusters with $n>1$ we only took the PDTP spectra shown in Fig. 4. The trends in these spectra are exactly analogous to those of the *X* and *I* state PDTP data above.

The question arises as to how one can extract reliable values for the adiabatic detachment energies (ADEs) of the *X*, *I*, and *II* states from the cluster spectra. For the *X* state, reasonably precise EAs can be obtained from the sharp peaks

($n=1$ and 2) and the shoulder ($n=3$) in the ZEKE spectra in Fig. 2. For $n>3$ EAs were estimated from the PDTP spectra by noting that the *X* state 0–0 transitions in the ZEKE spectra of $ArCl^-$ and Ar_2Cl^- are located where the respective PDTP spectrum reaches about 25% of its peak value. We therefore estimated the EA for all larger Ar_nCl clusters from this ''25% of maximum'' point of their PDTP spectra.

The same strategy was also applied to the *II* state: the *II* state 0–0 transitions were extracted from the PDTP spectra in Fig. 4 by using the $ArCl^-$ *II* state ZEKE spectrum with its known 0–0 transition[9] as a reference. The $ArCl^-$ PDTP spectrum was then superimposed. The comparison shows that for this particular cluster the 0–0 transition in the ZEKE spectrum is again located at the energy where the PDTP spectrum reaches 25% of its maximum value. For all the other *II* state PDTP spectra this value was taken as the reference point.

The location of the 0–0 transition in the ZEKE spectra of the *I* states is much less obvious, and a definite assignment can be given only for the $ArCl^-$ diatomic.[9] For $n=2$ and 3 the peaks in the ZEKE spectra of Fig. 2 closest to the positions corresponding to the ones predicted by our molecular dynamics calculations (Sec. IV) can be associated with the ADE to the *I* state. For the larger clusters, where only PDTP spectra are available, even such an estimate is no longer possible.

The resulting experimental electron affinities, *I* and *II* state 0–0 transitions (ADEs), as well as the $X-I$ and $X-II$ splittings obtained from the above procedures, are summarized in Table I together with estimated error bars. These will be discussed in greater detail together with the results from the simulated annealing MD calculations in Sec. V.

TABLE I. Experimental adiabatic electron affinities, excited state origins, and electronic state splittings for Ar_nCl. Estimated uncertainties (±) for state origins and splittings extracted from ZEKE and PDTP data are given in parentheses. All energies are in cm^{-1}.

n	EA[a] (X state origin)	I state origin[a]	Δ_{X-I}	II state origin[b]	Δ_{X-II}
0	29 138.59[c]	⋯	⋯	30 020.99[c,d]	882.4[d]
1	29 516.7 (2.0)	29 553.3 (2.0)	36.6 (4.0)	30 432.9 (3.0)	916.2 (5.0)
2	29 879.7 (2.0)	29 929.0 (15)	49.3 (17)	30 801.0 (50)	921.3 (52)
3	30 237.5 (10)	30 296.0 (15)	58.5 (25)	31 136.8 (50)	899.3 (60)
4	30 588.3 (50)	⋯	⋯	31 500.6 (50)	912.3 (100)
5	30 911.0 (50)	⋯	⋯	31 833.5 (50)	922.5 (100)
6	31 226.7 (50)	⋯	⋯	32 150.8 (50)	924.1 (100)
7	31 517.4 (50)	⋯	⋯	32 461.7 (50)	944.3 (100)
8	31 815.0 (50)	⋯	⋯	32 747.1 (50)	932.1 (100)
9	32 099.7 (50)	⋯	⋯	33 039.8 (50)	940.1 (100)
10	32 352.4 (50)	⋯	⋯	33 298.2 (50)	945.3 (100)
11	32 587.7 (50)	⋯	⋯	33 538.7 (50)	951.0 (100)
12	32 857.5 (50)	⋯	⋯	33 779.3 (50)	921.8 (100)
13	32 956.8 (50)	⋯	⋯	33 889.5 (50)	932.7 (100)
14	33 061.4 (50)	⋯	⋯	33 959.5 (50)	898.1 (100)
15	33 173.5 (50)	⋯	⋯	34 093.7 (50)	920.2 (100)

[a] $n=1-3$ extracted from ZEKE spectra (Fig. 2), $n=4-15$ from PDTP spectra (Fig. 3).
[b] $n=1$ from ZEKE spectrum (Ref. 9), $n=2-15$ from PDTP spectra (Fig. 4).
[c] Reference 29.
[d] Reference 28.

IV. SIMULATION OF EXPERIMENTAL RESULTS

The simulation methodology for our experimental results was discussed extensively in Refs. 10 and 11. In the first step, model potentials for the anion and neutrals have to be set up. Next, the minimum energy structures and their zero point energies are determined. From this information theoretical electron affinities and electronic state splittings can be extracted; these can be compared directly to the experimental data. Figure 1 illustrates how these theoretical and experimental quantities are related. The electron affinity $EA(Ar_nCl)$ of a Ar_nCl cluster can be determined via

$$EA(Ar_nCl) = EA(Cl) + \varepsilon_{an} - \omega_0^{an} - \varepsilon_X + \omega_0^X, \quad (3)$$

where EA(Cl) is the well-known electron affinity of atomic chlorine ($29\,138.59\,cm^{-1} = 3.612\,726\,eV$),[29] ε_{an} and ε_X represent the classical binding energy (well depth) of the anion and *X* state, respectively. ω_0^{an} and ω_0^X are the corresponding zero point energies. The experimental $X-I$ splitting, defined with respect to the anion and *X* vibrational ground states, can be obtained via

$$\Delta_{X-I} = \varepsilon_X - \omega_0^X - \varepsilon_I + \omega_0^I \quad (4)$$

and the $X-II$ splitting in a similar way by

$$\Delta_{X-II} = \varepsilon_X - \omega_0^X - \varepsilon_{II} + \omega_0^{II} + \Delta_{so}(Cl). \quad (5)$$

$\Delta_{so}(Cl)$ is the spin–orbit splitting of atomic chlorine ($0.1094\,eV = 882.4\,cm^{-1}$).[28] Evaluation of Eqs. (3)–(5) requires sufficiently accurate model potential functions. Using these, the minimum energy cluster geometries as well as zero point energies have to be determined.

A. Two-body potential functions

For representing the pairwise $ArCl^{(-)}$ interactions we used the optimized piecewise Morse—switching function—van der Waals (MSV) potentials from our earlier ZEKE study without further changes. The accuracy of these potential functions can be regarded as very high (absolute uncertainties: $\Delta R_m = \pm 0.08$ Å and $\Delta\varepsilon = \pm 0.6$ meV).[9] In addition to the Ar–Cl^- and Ar–Cl pair potentials, a potential function for Ar–Ar is required. As in one of our earlier studies[10] we used the Hartree–Fock dispersion (HFD-B2) potential of Aziz and Slaman ($R_m = 3.7565$ Å and $\varepsilon = 12.34$ meV).[30] Note that a slightly more precise Ar–Ar potential (HFDID1) has recently been published;[31] however, the simpler HFD-B2 potential is sufficiently accurate for our purposes here.

The pairwise additive approximation to the Ar_nCl^- bind-

ing energies was found by minimizing the additive potentials using the simulated annealing MD simulations described below via

$$\varepsilon_{an} = \min(V_{Ar-Cl^-} + V_{Ar-Ar}), \tag{6}$$

where

$$V_{Ar-Cl^-} = \sum_i V_{i0}(|\mathbf{r}_i - \mathbf{r}_0|) \tag{7}$$

and

$$V_{Ar-Ar} = \sum_{i<j} V_{ij}(|\mathbf{r}_i - \mathbf{r}_j|). \tag{8}$$

The sum is evaluated over all argon atoms; $\mathbf{r}_i$ and $\mathbf{r}_0$ denote the position of the ith argon atom and the chloride anion, respectively.

In the calculation of the Ar_nCl neutral potentials the open-shell nature of the chlorine atom has to be taken into account. We use a standard first-order perturbation theory treatment to describe the interaction of the open-shell chlorine atom with several argon atoms in terms of the two-body Ar–Cl potentials[9] as in our earlier work on Xe_nI, Ar_nI, and Ar_nBr clusters.[10,11,13] The resulting potentials are usually referred to as ''matrix additive.'' [3,32,33]

B. Many-body interactions

In the following we only give a very brief summary of the many-body interactions needed for modeling our experimental results. These were already discussed in detail in our earlier publications dealing with the Xe_nI^-, Ar_nI^-, and Ar_nBr^- systems.[10,11] Simplified pictorial representations of the most important effects are given in Fig. 5: We consider nonaddative induction {repulsion between induced dipoles on adjacent argon atoms [Fig. 5(a)] and charge-induced quadrupole effects}, charge-exchange quadrupole terms [Fig. 5(b)], charge-dispersion multipole interactions and the Axilrod–Teller triple–dipole effect [Fig. 5(c)]. Higher multipole three-body dispersion terms [e.g., the dipole–dipole–quadrupole interaction (DDQ)] as well as three-body exchange effects are neglected in our simulations, as they are thought to have only a minor influence on the EAs. Specific parameters used for the calculation of the different nonadditive effects can be found in Table II.[34–44]

C. Simulated annealing MD calculations

We use the same flexible simulated annealing MD algorithm as in our earlier ZEKE study on $Xe_nI^{(-)}$ clusters. It can be summarized as follows:[11] In the first step the initial positions of the argon atoms and chloride ion are chosen randomly inside a cubic box with edges of 6–18 Å length, depending on the cluster size. To prevent the evaporation of atoms which start in a highly repulsive region of the potential energy surface, the minimum distance allowed between two atoms in the box is 3.2 Å. In the second step the cluster is ''quenched,'' i.e., kinetic energy is rapidly removed by rescaling the velocities of the atoms. As a result, the cluster quickly ends up in a minimum on the potential energy surface. In the third step, a ''simulated annealing'' procedure is performed, starting with the minimum energy configuration of the previous step. A randomly selected amount of kinetic

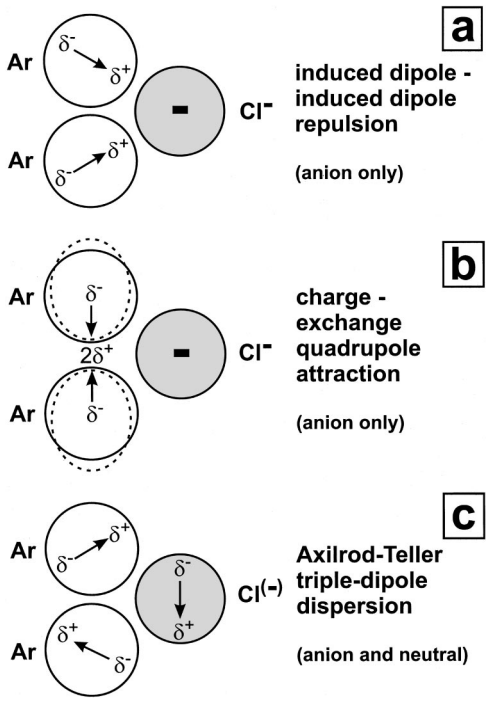

FIG. 5. ''Cartoons'' of selected many-body effects for $Ar_2Cl^{(-)}$. (a) Nonadditive induction (repulsion between induced dipoles); (b) attraction between the chloride charge and the exchange quadrupole of two argon atoms; (c) Axilrod–Teller triple–dipole dispersion (repulsive for the triangular arrangement shown here, but attractive for the linear configuration). The most important effect is the destabilization of the anion cluster by nonadditive induction.

TABLE II. Atomic dipole (α_d) and quadrupole polarizabilities (C), effective numbers of electrons (N), and triple–dipole coefficients (C_9) for the Ar–Ar–Cl^- and Ar–Ar–Cl interactions needed in the simulated annealing MD simulations. Values for the quadrupole polarizabilities are based on Buckingham's definition ($C = 0.5 \cdot \alpha_q$) (Ref. 34). For the description of the dispersion induced dipole and quadrupole moments $C_\mu = 1252\, e a_0^8$ and $C_\Theta = 208.6\, e a_0^8$ were used, respectively (Refs. 10, 11). Calculated β values for the Ar_2 exchange quadrupole are available from Hutson and co-workers who used 0.936 $Å^{-1}$ (Ref. 42) and 0.965 $Å^{-1}$ (Ref. 43) for Ar_2HF and Ar_2HCl. These values were obtained from a SCF calculation and distributed multipole analysis of the Ar_2 quadrupole moment (Ref. 44). In the simulations here, we use $\beta = 0.927$ $Å^{-1}$ which results in a better overall agreement of experimental and calculated electron affinities and is still well within the uncertainties of Hutson's calculated β value.

Atom	$\alpha_d(a_0^3)$	$C(a_0^5)$	N	C_9 (eV Å^9)
Ar	11.08[a]	26.39[b]	5.9[c]	⋯
$C1^-$	36.997[d]	199.85[d]	5.9[c]	128.2[e]
Cl	14.63[f]	⋯	4.2[c]	58.1

[a]Reference 35.
[b]Reference 36.
[c]Reference 37.
[d]Reference 38. These calculated dipole and quadrupole polarizabilities for the chloride anion are in excellent agreement with the values $\alpha_d = 36.86\, a_0^3$, $\alpha_d = 37.43\, a_0^3$, $C = 188.1\, a_0^5$, and $C = 189.4\, a_0^5$ calculated in Ref. 39.
[e]This is in good agreement with Chalasinski's *ab initio* value $C_9(Ar_2Cl^-) = 116.4$ eV Å^9 which represents a lower bound to the true value, as the basis set used in that study is not completely saturated (Ref. 14).
[f]Spherically averaged value calculated in Ref. 40. This agrees very well with $\alpha_d = 14.73\, a_0^3$ from Ref. 41.

energy, typically between 5% and 35% of the classical binding energy, is added. Next, the system is gradually cooled down by removing kinetic energy until the lowest energy state is reached. Finally, in the fourth step, a gradient minimization algorithm is used to locate the minimum energy structure of the annealing run more precisely. These four steps are repeated up to 1000 times, depending on the cluster size and the potential model applied. This allows us to obtain a complete survey of all the relevant global and local cluster minima.

As in our earlier study of Xe_nI^- clusters, we found that for Ar_nCl^- clusters with $n \leqslant 12$, rapidly quenching a large enough number of random starting configurations—without an additional annealing step—also found the global minimum and the most important local minima on the potential energy surface, though in a much shorter time. This was therefore the method of choice for determining the minimum energy structures of the smaller clusters.

To obtain the minimum energy structures of the neutrals accessed by photodetachment, the optimized anion geometry is relaxed on the appropriate neutral surface. Finally, zero point energies for the anion and neutral clusters are determined using the ''anharmonic normal mode analysis'' described in our earlier paper,[10] which was shown to yield good agreement with the results from semiclassical initial value representation methods.[45] Electron affinities and the other detachment energies can then be calculated via Eq. (3) and the analogous expressions for the *I* and *II* states.

The above procedure yields global and local minima on the cluster potential energy landscape. In order to explore possible effects of finite temperature, simulations were also performed using a standard constant temperature MD approach.[46] For these calculations, the velocities of all particles were periodically rescaled by a factor $(T_{\text{targ}}/\langle T\rangle)^{1/2}$, where T_{targ} is the desired temperature in the respective simulation ($\leqslant$60 K in the simulations presented here), and $\langle T\rangle$ represents the instantaneous average kinetic temperature of the system obtained from

$$\langle T\rangle = \frac{2}{3Nk_B}\langle E_{\text{kin}}\rangle. \tag{9}$$

Here N is the total number of atoms in the cluster, k_B is Boltzmann's constant, and E_{kin} is the average kinetic energy calculated from the preceding MD step. The evolving anion cluster structures in these finite temperature MD runs were analyzed as a function of time and then compared to the global and local minimum energy structures obtained at 0 K.

V. ANALYSIS AND DISCUSSION

A. Global and local minimum energy structures at 0 K

We start by discussing the anion and neutral minimum energy structures (at 0 K) found from the above MD simulation procedure. After that, our experimental findings for the cluster-dependent EAs are presented, and these are compared with EAs calculated from the model potentials with and without inclusion of nonadditive effects.

In Fig. 6 we show the global minimum energy structures for the Ar_nCl^- clusters with $n=2-15$ obtained when all many-body terms are included. In all the clusters the argon atoms are grouped around the central chloride anion, allowing the maximum number of Ar–Cl^- bonds to be formed. (Note that each of these bonds is more than five times stronger than a bond between two argon atoms.) Next, the argon atoms are grouped in such a way that the number of Ar–Ar bonds is maximized. The $n=12$ cluster forms an icosahedron of argon atoms around the central chloride anion. All clusters with $n<12$ can be seen as fragments derived from this icosahedral structure. Thus, for example, the cluster with $n=6$ represents half an icosahedral shell.

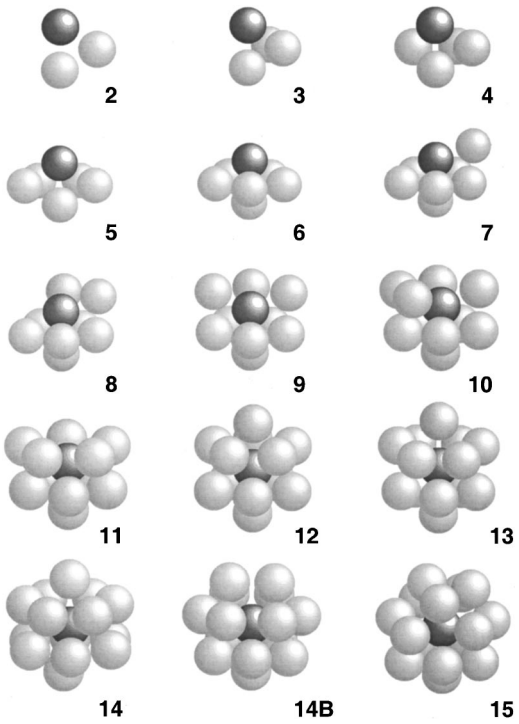

FIG. 6. Global minimum energy structures of Ar_nCl^- anion clusters ($n=2-15$) at 0 K. All structures were obtained using the MSV two-body $ArCl^{(-)}$ pair potentials including all many-body options. For $n=14$ two nearly isoenergetic isomers (''14'' and ''14B'') with different structures exist. The argon atoms and the chloride ion are shown with less than their full van der Waals radii for the sake of clarity. See the text for details.

The same notation is used to characterize the clusters based on the pictorial representation of Fig. 6 as in our earlier paper on Xe_nI^- clusters.[11] The icosahedron can be referred to as ''1–5–5–1,'' where the first ''1'' denotes the single argon at the bottom, the ''5'' is the lower 5-ring structure, the second ''5'' represents the five atoms of the upper ring structure and the final ''1'' is the single argon atom at the top. The $n=6$ ''half-shell'' cluster is termed ''1–5–0–0,'' and an icosahedral cluster with one additional atom in the second solvent-shell is labeled ''(1–5–5–1)–1,'' where the parentheses denote a closed first solvent shell.

For $n=14$ there are two almost isoenergetic minimum energy structures of different geometry. Both are characterized by a closed-shell of argon atoms. Structure ''14'' represents a bicapped hexagonal antiprism, and can be described as ''1–6–6–1,'' i.e., there are two 6-rings, each of them carrying an additional argon atom on top. The second struc-

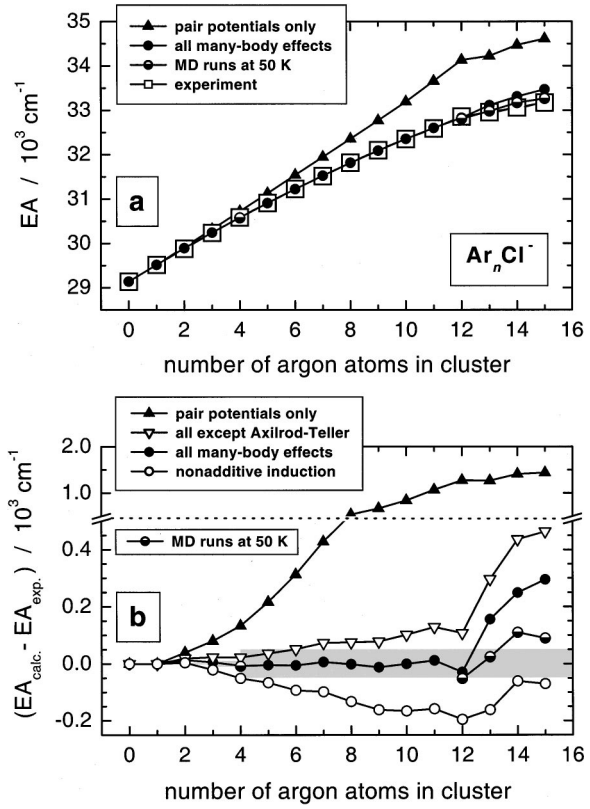

FIG. 7. (a) Comparison of size-dependent experimental electron affinities with those calculated from different potential models. □; experimental EAs from Table I; ▲: pair potential (P) for anion, matrix additive potential (M) for the *X* state; ●: P+nonadditive induction (I)+exchange/dispersion multipole-charge interactions (C)+Axilrod–Teller (A) for anion, M and A potential for *X* state; half-filled circles: EAs estimated from MD runs at 50 K (see Table III and text). (b) Differences between calculated and experimental electron affinities: ▲, ● and half-filled circles as in (a), ▽:P+I+C for anion, M for *X* state; ○:P+I for anion, M for *X* state. Uncertainties of the experimental EAs from Table I are shown as gray-shaded regions.

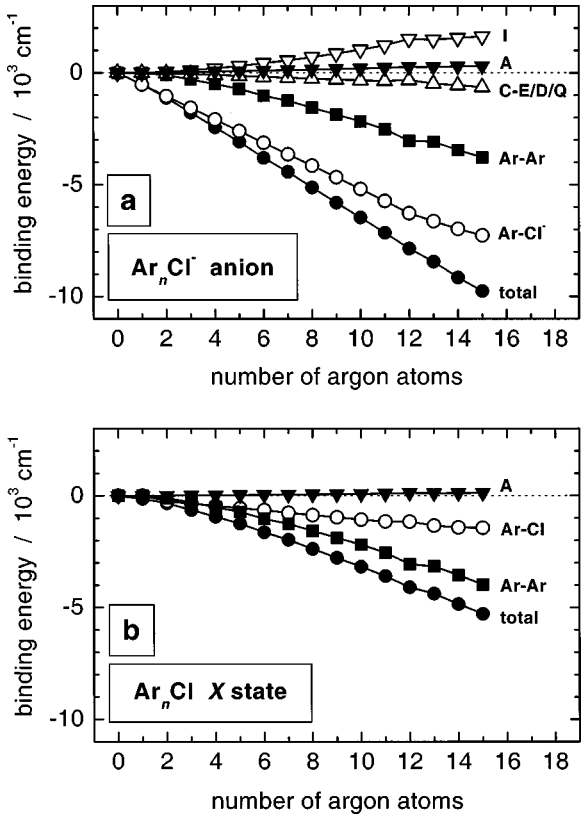

FIG. 8. Contributions to the total classical binding energies for the Ar_nCl^- anion clusters (a) and the Ar_nCl *X* state clusters (b) extracted from simulated annealing MD calculations including all nonadditive potential terms. ●: total classical binding energy; ○:$ArCl^-$(ArCl) contribution for anion (neutral); ■: Ar–Ar contribution; △: *combined* charge-exchange quadrupole, charge-dispersion dipole, and charge-dispersion quadrupole contributions (C-E/D/Q); ▼: Axilrod–Teller triple–dipole dispersion; ▽: nonadditive induction.

ture, ''14B,'' is derived from a decahedron with two additional argon atoms squeezed in between its two halves. The latter structure can be termed as ''1–5–6–2,'' i.e., compared to the $n=13$ cluster an additional argon atom is placed on top of the 6-ring. The global minimum energy structures for $n=12-14$ at 0 K all clearly possess a closed shell of argon atoms.

B. Electron affinities and neutral *X–I*, *X–II* state splittings

The experimental electron affinities as a function of cluster size are shown in Fig. 7(a) (□). The electron affinities increase with *n* due to the stronger stabilization of the anion relative to the *X* state by the Ar atoms. The EA curve shows a steadily decreasing slope toward large *n*, with a particularly significant drop above $n=12$ (see also Table I). This will be discussed in more detail in Sec. V C.

In Figs. 7(a) and 7(b), the experimental EA's are compared to results from simulations incorporating various many-body corrections, with Fig. 7(b) showing the *differences* between the calculated and experimental values. Details about the influences of individual terms were discussed in more detail in our earlier publications.[10,11,13] In analogy to those investigations we find that when many-body effects are neglected, the calculated EAs are significantly larger than the experimental values (e.g., $+1273\ cm^{-1}$ at $n=12$). These results are shown both in Figs. 7(a) and 7(b) (▲). The most important individual nonaddictive effect is many-body induction in the anion [○, Fig. 7(b)], which leads to a significant decrease of the EAs mainly due to repulsion of induced dipoles on adjacent argon atoms. Adding the charge-exchange quadrupole, the charge-dispersion multipole interactions [▽, Fig. 7(b)] and finally the Axilrod–Teller triple–dipole dispersion leads to size-dependent EAs [●, Figs. 7(a) and 7(b)] which are very close to the experimental values up to $n=12$. However, for $n>12$ we observe deviations which are larger than the experimental uncertainties stated in Table I [shaded region in Fig. 7(b)]. This point will be discussed in Sec. V C.

The contributions of the various nonaddictive effects to the total classical binding energy at the optimized equilibrium structure of each cluster are shown in Fig. 8(a) for the Ar_nCl^- anions and in Fig. 8(b) for the Ar_nCl *X* states. A complete compilation of individual potential term contributions and cluster energies can be obtained from the authors upon request. The observed trends are largely consistent with our earlier results for $Xe_nI^{(-)}$, $Ar_nI^{(-)}$, and $Ar_nBr^{(-)}$, where

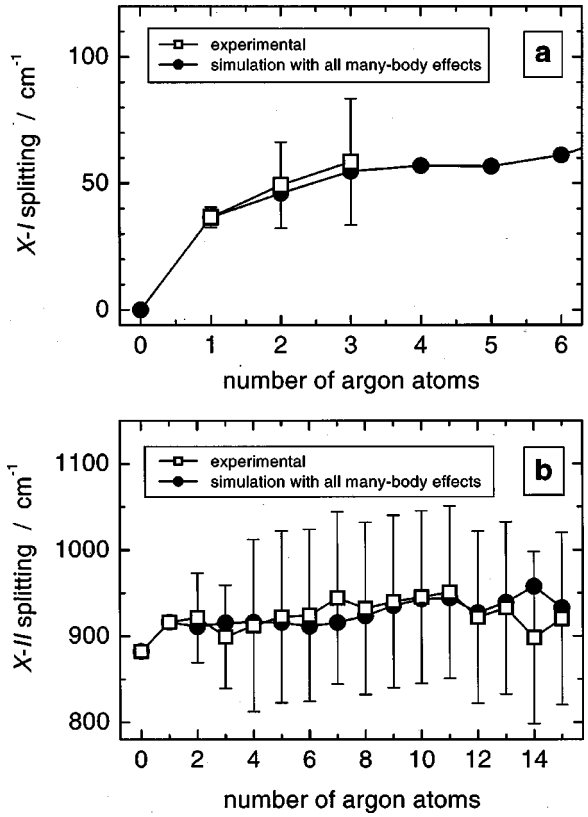

FIG. 9. Experimental and calculated neutral state splittings. (a) $X-I$ splitting; (b) $X-II$ splitting. □: experiment (Table I); ●:simulation including all many-body effects. Uncertainties of the experimental splittings from Table I are included as error bars.

many-body induction in the anion cluster was also found to be the largest nonaddictive effect.[10,11,13]

In Fig. 9 the splittings for the different neutral states obtained from experiment (Table I) are compared with the simulation results employing the potential models with all many-body options included. The $X-I$ state splittings are shown in Fig. 9(a). Experimental values for $n=2$ and 3 can only be estimated with the aid of our MD simulations. For the larger clusters such an estimate is not possible, because the X and I state features are not as clearly separated as, for example, in our earlier study on $Xe_nI^{(-)}$ where the splittings were much larger.[11] In Fig. 9(b) the results for the $X-II$ splittings are shown. Again good agreement between experiment and simulation is found when taking the experimental error bars into account.

C. Constant temperature MD simulations for $T \leqslant 60$ K

In Sec. III we already noted the discrepancies between our experimental and simulated EAs for clusters with $n>12$. The experimentally observed sharp decrease in slope of the EA curve (Fig. 7) and the very steep slope of the PDTP spectra for $Ar_{13}Cl^-$ in Figs. 3 and 4 suggest a shell closing at $n=12$.[13] In this case, additional argon atoms would go into the second shell on top of the surface of the icosahedron, leading to a smaller stabilization of the anion clusters relative to the X state since argon atoms in the second shell are much further (5–6 Å) away from the chloride core. Such an interpretation is at first sight not in agreement with the minimum energy structures discussed above.

These discrepancies for $n>12$ could not be resolved by any adjustment of the potential functions. The bounds of such a variation are very restricted: the two-body $Ar-Cl^{(-)}$ potentials have estimated absolute uncertainties of $\Delta R_m = \pm 0.08$ Å and $\Delta\varepsilon = \pm 0.6$ meV.[9,28] Using modified potentials with slightly different values for R_m and ε (even going beyond the specified error limits) brought no change in slope of the EA(n) curve above $n=12$. The Ar–Ar potential is highly accurate.[30,31] In addition, the parameters entering the expressions for the nonaddictive effects (e.g., those in Table II) are also known with considerable precision.

The most severe approximation in our simulation procedure is the assumption of a 0 K cluster temperature. While the exact temperature of the cold Ar_nCl^- clusters in our photodetachment experiments is unknown, the ''hot band'' congestion in the spectra (see, e.g., $n=3$ in Fig. 2) suggests a fair amount of internal excitation. We have tried to estimate the influence of such an excess energy on the anion cluster structures by performing additional MD calculations for selected Ar_nCl^- species ($n=4,12-15$) at temperatures up to 60 K (Sec. IV C).

In these simulations we followed the individual trajectories of each atom in the cluster over an extended period of time (e.g., 500 ps). The first interesting result in all of these runs was that, despite considerable structural fluctuations, the chloride anion always remained in the center of the cluster for $n=12-15$. This means that even at the elevated temperatures considered here ''surface structures'' are not populated. In order to follow the temporal evolution of the clusters' structures for different n in more detail, it is useful to monitor each $Ar-Cl^-$ distance as a function of time. Argon atoms at separations above 5.30 Å are considered to be in the second solvent shell. This distance was deduced on the basis of several ''0 K'' structures with second shell argon atoms, and the following qualitative analysis is not very sensitive to the exact value. All argon atoms at distances shorter than 5.30 Å are regarded as belonging to the first solvent shell. As a reasonable estimate we assume a fixed temperature of 50 K for all clusters. At even higher temperatures the anion clusters dissociate and would therefore not be stable during the several tens of microseconds required to transit our mass spectrometer before photodetachment.

Results of our MD simulations are shown in Fig. 10. The clusters with $n=4$ (■) and 12 (○) have all of their argon atoms in the first solvent shell around the Cl^- anion for most of the time at 50 K. In this case there is enough space for all of the argon atoms to keep their energetically most favorable position close to the central Cl^- anion despite considerable thermal fluctuations. The picture dramatically changes when only one more argon atom is added. Starting with $n=13$ (▼), for about 50% of the time one of the 13 argon atoms is already in the second solvent shell, due to steric congestion around the central chloride anion. While such a cluster at this temperature has a highly fluxional structure, it can be described on average as a distorted 12-atom-icosahedron with the additional argon atom bouncing around on the outside of the first shell. For the larger $n=14$ (△) and 15 (◆) clusters,

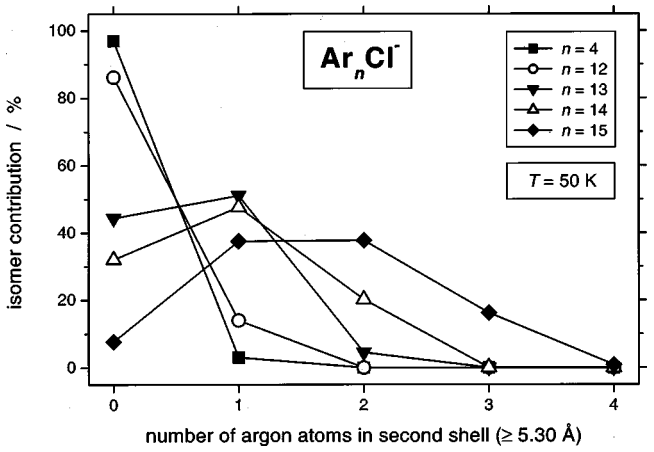

FIG. 10. Contribution of different isomer classes for four different Ar_nCl^- clusters ($n=4$, 12–15) as deduced from the temporal evolution of the cluster structures in MD runs at 50 K. Isomers with 0–4 argon atoms in the second solvent shell (≥5.30 Å) are shown.

structures with two and three second shell argon atoms become increasingly important (Table III).

How do the EAs of internally excited clusters differ from those of the global minimum energy structures? To answer this question it is very helpful to consider the EAs of the global and several local minimum energy structures for each cluster. For clusters with $n \leqslant 12$ the MD runs at 50 K indicate that one also has to consider those structures which still have all argon atoms in contact with the Cl^- anion (as the global minima in Fig. 6) *but* fewer Ar–Ar bonds. A comprehensive survey of such structures for several cluster sizes showed that local minima of this kind are typically destabilized by roughly 80 cm^{-1} per broken Ar–Ar bond relative to the global minimum. The key point is, however, that the EAs for all these local minimum structures are nevertheless *almost identical* to that of the global minimum (e.g., within 10 cm^{-1} for Ar_8Cl^-), because the corresponding X state structures accessed by photodetachment are destabilized by nearly the same amount. In terms of the EAs it therefore does not matter which of the isomers is detached as long as all argons are in contact with the Cl^-. Thus, it can be expected that our calculated EAs of the global minimum structures for $n \leqslant 12$ in Fig. 6 will yield reliable EAs close to the experimental values even if the clusters in the experiment have some degree of internal excitation. The only effect of the population of local isomers with a different arrangement of argon atoms in the first solvent shell will be a slight broadening of the spectra, which is consistent with Fig. 2.

TABLE III. EA estimates for Ar_nCl^- isomer mixtures with $n=4$ and 12–15. i represents the number of argon atoms in the second shell for each cluster. For the clusters with $i=0$ (no argon in the second shell) the EAs are identical to those in Fig. 7 (●). For clusters with $i>0$ the EAs have been estimated on the basis of appropriate local minimum energy structures obtained from our simulated annealing calculations. The total EA in the last column represents the sum of the individual isomer EAs weighted by their respective contributions (see also Fig. 10).

n	i	EA of Ar_nCl isomer	Contribution	Total EA
4	0	30 582	0.9696	30 574
	1	30 304	0.0304	
12	0	32 829	0.8614	32 806
	1	32 660	0.1386	
13	0	33 113	0.4439	32 981
	1	32 889	0.5111	
	2	32 720	0.0450	
14	0	33 310	0.3204	33 171
	1	33 173	0.4770	
	2	32 949	0.2020	
	3	32 780	0.0006	
15	0	33 468	0.0768	33 263
	1	33 370	0.3750	
	2	33 233	0.3776	
	3	33 009	0.1621	
	4	32 840	0.0085	

The picture is totally different for clusters with $n>12$. Structures with one or more argon atoms in the second shell detach at significantly lower energies than the respective global minimum structures in Fig. 6. For each argon atom, which is moved from the first to the second shell, the EA of the cluster decreases by 100–250 cm^{-1}. We have estimated the EAs of isomer mixtures for clusters with $n=4$ and 12–15. For that we took the EA of the global minimum and estimated the EAs of respective local minimum energy structures with up to four atoms in the second shell, using information on the cluster energetics from our simulations. The isomer EAs were then weighted according to their contribution obtained from the MD simulations at 50 K (Fig. 10). Values for the EAs determined this way are given in Table III and are also included in Fig. 7 as half-filled circles. For $n=13$–15 the agreement with the experimental EAs is now much better and within or close to the experimental error bars. The EAs for $n=12$ and especially $n=4$ remain virtually unchanged as isomers with argon atoms in the second shell play only a small role in these cases (Fig. 10). It therefore appears as if some degree of internal excitation of the Ar_nCl^- clusters is the key for understanding the experimentally observed change in slope of the EA curve above $n=12$.

D. Comparison with other systems

We conclude our discussion by comparing the present results with our earlier data on other polyatomic rare gas halide systems. As discussed in Sec. V B, neglect of the many-body interactions leads to a large deviation from the experimental EA, e.g., +1273 cm^{-1} for $Ar_{12}Cl$. This can be compared with values from our earlier ZEKE studies; for $Ar_{12}I$ the difference is +560 cm^{-1},[10] whereas for $Xe_{12}I$ one obtains +2313 cm^{-1}.[13] The deviation between Xe_nI and Ar_nI is considerable because of the much larger nonaddictive induction effect due to the high polarizability of the xenon atoms. In the case of the Ar_nX clusters the chlorine species show the larger deviation, as the Ar–Cl^- distance in the clusters is shorter than for Ar–I^-, and thus the nonaddictive induction effect is stronger in Ar_nCl^-. The observed trends do not change, even when the values are scaled by the change of the electron affinities $[EA(n=12)-EA(n=0)]$, which is 3720 cm^{-1} for Ar_nCl, 2230 cm^{-1} for Ar_nI, and 4920 cm^{-1} for Xe_nI clusters.[13]

The two-body potential functions and many-body parameters used in the present simulations of the Ar_nCl^- systems are the most accurate applied so far. Therefore we believe that the many-body effects for this rare gas halide system can be particularly well characterized in this study.

In the Xe_nI^- system the ZEKE and PDTP spectra for the *X* and *I* states were influenced by contributions of ''charge-transfer-to-solvent (CTTS)'' states.[13] These CTTS states are supported by the large polarizability of the xenon atoms and were first observed by Cheshnovsky and co-workers.[47,48] In a complementary PES study from our lab the influence of the CTTS states was quantified, which led to refined values of the EAs of Ref. 11. In the Ar_nCl^- systems studied here (and also for Ar_nI^-) such CTTS states are not likely to be present, because the argon atoms are much less polarizable.

VI. CONCLUSIONS

ZEKE and PDTP spectroscopy of the Ar_nCl^- anion clusters with $n=2-15$ has yielded adiabatic electron affinities and splittings between the neutral electronic states accessed by photodetachment. With the aid of simulated annealing MD calculations of the cluster structures we were able to demonstrate that EAs calculated from pair potentials alone (i.e., without any nonaddictive effects included) drastically overestimate the experimental values. The dominant many-body effect is nonaddictive induction, specifically the repulsion between charge-induced dipoles on adjacent argon atoms. This effect alone accounts for most of the discrepancy between ''additive'' and experimental EAs, but overcorrects the deviations observed for pure pair potentials. Additional inclusion of the *attractive* charge-exchange quadrupole term recovers this overcorrection and brings the calculated EAs even closer to experiment. The remaining discrepancies between the experimental and simulated ''0 K'' EAs for clusters with $n>12$ can be very likely attributed to the influence of the finite temperature of the anion clusters in our experiment. We demonstrated this by constant temperature MD simulations at $T\leqslant 60$ K, which showed that the population of structures with one or several argon atoms in the second solvent shell can have a visible influence on the measured EA at elevated temperatures.

Qualitatively, our findings about the relative importance of the individual many-body effects in the $Ar_nCl^{(-)}$ system are completely consistent with our earlier results for $Xe_nI^{(-)}$, $Ar_nI^{(-)}$, and $Ar_nBr^{(-)}$ clusters.[10,11,13] Note that many-body induction has been recognized recently as particularly important for a correct description of other charged systems, as, e.g., the structure of Ar_n^+ clusters.[49] Some caution is advised when drawing conclusions about the exact influence of other many-body contributions from our experiments. Effects which are present in both the anion and the neutral (like the Axilrod–Teller triple–dipole interaction, three-body exchange contributions, and higher-order multipole dispersion terms) at least partially cancel out in EA measurements, and we are therefore not very sensitive to them. Additional high resolution spectroscopic experiments on related systems coupled with *ab initio* calculations would be very useful in this respect. We therefore hope that our results will stimulate further experimental and theoretical studies of nonadditive interactions.

ACKNOWLEDGMENTS

This research is supported by the Air Force Office of Scientific Research under Grant No. F49620-00-1-0145. T. Lenzer is grateful to the Deutsche Forschungsgemeinschaft for a postdoctoral fellowship, and M. R. Furlanetto thanks the National Science Foundation for a predoctoral fellowship. We also thank J. Troe for providing computer time needed for the simulated annealing calculations, and R. B. Gerber, P. Jungwirth, A. Krylov, C. C. Martens, and Z. Li for providing early versions of the molecular dynamics programs. Helpful discussions with M. Okumura on possible influences of internal cluster excitation in our experiments are gratefully acknowledged.

[1] T. Kühne, R. Küster, and P. Vöhringer, Chem. Phys. **233**, 161 (1998).
[2] M. E. Fajardo and V. A. Apkarian, J. Chem. Phys. **89**, 4102 (1988).
[3] W. G. Lawrence and V. A. Apkarian, J. Chem. Phys. **101**, 1820 (1994).
[4] S. Nandi, A. Sanov, N. Delaney, J. Faeder, R. Parson, and W. C. Lineberger, J. Phys. Chem. A **102**, 8827 (1998).
[5] B. J. Greenblatt, M. T. Zanni, and D. M. Neumark, Faraday Discuss. **108**, 101 (1997).
[6] Y. Zhao, I. Yourshaw, G. Reiser, C. C. Arnold, and D. M. Neumark, J. Chem. Phys. **101**, 6538 (1994).
[7] I. Yourshaw, T. Lenzer, G. Reiser, and D. M. Neumark, J. Chem. Phys. **109**, 5247 (1998).
[8] T. Lenzer, M. R. Furlanetto, K. R. Asmis, and D. M. Neumark, J. Chem. Phys. **109**, 10754 (1998).
[9] T. Lenzer, I. Yourshaw, M. R. Furlanetto, G. Reiser, and D. M. Neumark, J. Chem. Phys. **110**, 9578 (1999).
[10] I. Yourshaw, Y. Zhao, and D. M. Neumark, J. Chem. Phys. **105**, 351 (1996).
[11] T. Lenzer, M. R. Furlanetto, N. L. Pivonka, and D. M. Neumark, J. Chem. Phys. **110**, 6714 (1999).
[12] H. Margenau and N. R. Kestner, *Theory of Intermolecular Forces* (Pergamon, Oxford, 1969).
[13] N. L. Pivonka, T. Lenzer, M. R. Furlanetto, and D. M. Neumark, Chem. Phys. Lett. **334**, 24 (2001).
[14] R. Burcl, S. M. Cybulski, M. M. Szczesniak, and G. Chalasinski, J. Chem. Phys. **103**, 299 (1995).
[15] A. I. Krylov, R. B. Gerber, and R. D. Coalson, J. Chem. Phys. **105**, 4626 (1996).
[16] K. M. Christoffel, A. L. Trayanov, and M. G. Prisant, J. Chem. Phys. **101**, 4418 (1994).
[17] A. L. Trayanov and M. G. Prisant, J. Chem. Phys. **101**, 4433 (1994).
[18] J. G. McCaffrey, H. Kunz, and N. Schwentner, J. Chem. Phys. **96**, 155 (1992).
[19] F. Y. Naumkin and D. J. Wales, Chem. Phys. Lett. **290**, 164 (1998).
[20] A. Rohrbacher, J. Williams, and K. C. Janda, Phys. Chem. Chem. Phys. **1**, 5263 (1999).
[21] A. Rohrbacher, K. C. Janda, L. Beneventi, P. Casavecchia, and G. G. Volpi, J. Phys. Chem. A **101**, 6528 (1997).
[22] C. R. Bieler, D. D. Evard, and K. C. Janda, J. Phys. Chem. **94**, 7452 (1990).
[23] V. Distelrath and U. Boesl, Faraday Discuss. **115**, 161 (2000).
[24] T. N. Kitsopoulos, I. M. Waller, J. G. Loeser, and D. M. Neumark, Chem. Phys. Lett. **159**, 300 (1989).
[25] C. C. Arnold, Ph.D thesis, University of California, Berkeley, 1994.
[26] T. Baer, W. B. Peatman, and E. W. Schlag, Chem. Phys. Lett. **4**, 243 (1969).
[27] R. Spohr, P. M. Guyon, W. A. Chupka, and J. Berkowitz, Rev. Sci. Instrum. **42**, 1872 (1971).
[28] V. Aquilanti, D. Cappelletti, V. Lorent, E. Luzzatti, and F. Pirani, J. Phys. Chem. **97**, 2063 (1993).
[29] U. Berzinsh, M. Gustafsson, D. Hanstorp, A. Klinkmüller, U. Ljungblad, and A.-M. Martensson-Pendrill, Phys. Rev. A **51**, 231 (1995).
[30] R. A. Aziz and M. J. Slaman, Mol. Phys. **58**, 679 (1986).

[31] R. A. Aziz, J. Chem. Phys. **99**, 4518 (1993).
[32] K. M. Sando, G. J. Erickson, and R. C. Binning Jr., J. Phys. B **12**, 2697 (1979).
[33] G. J. Erickson and K. M. Sando, Phys. Rev. A **22**, 1500 (1980).
[34] A. D. Buckingham, Adv. Chem. Phys. **12**, 107 (1967).
[35] A. Kumar and W. J. Meath, Mol. Phys. **54**, 823 (1985).
[36] C. Hättig and B. A. Heß, J. Phys. Chem. **100**, 6243 (1996).
[37] E. A. Mason and E. W. McDaniel, *Transport Properties of Ions in Gases* (Wiley, New York, 1988).
[38] C. Hättig and B. A. Heß, J. Chem. Phys. **108**, 3863 (1998).
[39] V. Kellö and A. J. Sadlej, Chem. Phys. **157**, 123 (1991).
[40] K. Andersson and A. J. Sadlej, Phys. Rev. A **46**, 2356 (1992).
[41] M. Medved, P. W. Fowler, and J. M. Hutson, Mol. Phys. **98**, 453 (2000).
[42] A. Ernesti and J. M. Hutson, Phys. Rev. A **51**, 239 (1995).
[43] A. R. Cooper and J. M. Hutson, J. Chem. Phys. **98**, 5337 (1993).
[44] A. R. Cooper, Ph.D. thesis, Durham University, 1992.
[45] M. L. Brewer, J. S. Hulme, and D. E. Manolopoulos, J. Chem. Phys. **106**, 4832 (1997).
[46] M. P. Allen and D. J. Tildesley, *Computer Simulation of Liquids* (Oxford University, Oxford, 1987).
[47] I. Becker, G. Markovich, and O. Cheshnovsky, Phys. Rev. Lett. **79**, 3391 (1997).
[48] I. Becker and O. Cheshnovsky, J. Chem. Phys. **110**, 6288 (1999).
[49] N. L. Doltsinis, P. J. Knowles, and F. Y. Naumkin, Mol. Phys. **96**, 749 (1999).